Nanoscale

PAPER

View Article Online
View Journal | View Issue

Cite this: *Nanoscale*, 2019, **11**, 17782

MOF-based fibrous membranes adsorb PM efficiently and capture toxic gases selectively†

Xiaoyu Wang,[a] Wenshi Xu,[a,b] Jin'ge Gu,[a,b] Xiaoying Yan,[a] Yi Chen,[c] Mengyu Guo,[a] Guoqiang Zhou,[b] Shengrui Tong,[c] Maofa Ge,[c] Ying Liu*[a] and Chunying Chen*[a]

Air pollution is harmful to the functioning of the lungs, heart, and brain even at low concentrations of particle matter (PM) and toxic gases. Purification methods and materials have made tremendous progress to improve the purity of air to adhere to national quality standards. Metal–organic frameworks (MOFs) have an excellent gas adsorption capacity due to their high specific surface area and porous structure, but the intrinsic fragility of MOF crystals limits their application. In this study, we selected appropriate organic ligands to prepare MOF-surface-grown fibrous membranes using an electrospinning technique, which have an excellent ability to adsorb PM and capture toxic gases selectively. The efficiency of the MOF-surface-grown fibrous membranes to remove PM reached 99.99%, even for fine PM. More importantly, under low partial pressure and complex gas composition conditions, the fibrous membrane was able to selectively adsorb SO_2. The concentration of SO_2 dropped from 7300 ppb to 40 ppb. Interestingly, the MOF-surface-grown fibrous membrane had a higher purification capacity toward O_3 than toward SO_2. The concentration of O_3 rapidly dropped from 3000 ppb to 7 ppb, which was far below national air quality standards (81 ppb). The MOF-surface-grown fibrous membrane was able to adsorb toxic atmospheric gases selectively, while not being influenced by the presence of other gases, such as CO_2 and O_2. MOF-based fibrous membranes prepared using a simple and inexpensive electrospinning technique have wide potential for practical use in the field of environmental protection and air purification.

Received 9th July 2019,
Accepted 2nd September 2019

DOI: 10.1039/c9nr05795a

rsc.li/nanoscale

Introduction

Air pollution is a major factor affecting public health. In 2015, air pollution was responsible for 6.4 million deaths worldwide. About 2.8 million people died from indoor air pollution, and 4.2 million people suffered from environmental air pollution.[3] Particle matter (PM) and toxic gases such as sulfur dioxide (SO_2) and ozone (O_3) are the main pollutants, which cause pulmonary and cerebrovascular diseases when their concentration exceeds the safety range.[1–3] PM, especially ultrafine particles, can be deposited in the brain, thereby increasing the risk of neuroinflammation and Alzheimer's disease.[4,5] SO_2 and O_3 cause strong irritation in the respiratory tract and lungs.[6–8] At high concentrations, there is considerable evidence to support that SO_2 and O_3 can cause aggravation of asthma and pulmonary inflammation by inducing bronchoconstriction and eosinophilia.[9–12] According to World Health Organization (WHO) air quality standards,[3] the concentrations of SO_2, O_3, and $PM_{2.5}$ should be maintained below 125 μg m^{-3} (48 ppb), 160 μg m^{-3} (81 ppb), and 25 μg m^{-3} used as interim targets, respectively. Therefore, methods of air purification capable of filtering PM and adsorbing toxic gases have been widely investigated.

Electrospinning is a fascinating technique used to prepare porous fibrous membranes and has been extensively used in environmental protection and in biomedicine, catalysis, and photoelectricity.[13–16] Although electrospun fibrous membranes have a high efficiency for filtering PM, their capacity for adsorbing toxic gases is low. Metal–organic frameworks (MOFs), resulting from the coordination of metals and organic ligands, have attracted much attention because of their ultrahigh porosity, excellent gas storage and separation capacity, and functional surface area.[17–20] However, as an MOF is an unstable crystal, it is difficult to formulate it into films, which restricts its potential applications. Some methods have been

[a]*CAS Key Laboratory for Biomedical Effects of Nanomaterials and Nanosafety & CAS Center for Excellence in Nanoscience, National Center for Nanoscience and Technology of China, Beijing 100190, China. E-mail: chenchy@nanoctr.cn, liuy@nanoctr.cn*
[b]*Key Laboratory of Medicinal Chemistry and Molecular Diagnosis of Ministry of Education, College of Chemistry and Environmental Science, Hebei University, Baoding, 300401, China*
[c]*Beijing National Laboratory for Molecular Sciences, State Key Laboratory for Structural Chemistry of Unstable and Stable Species, Institute of Chemistry, Chinese Academy of Sciences, Beijing 100190, China*
†Electronic supplementary information (ESI) available. See DOI: 10.1039/c9nr05795a

proposed to add MOFs to a polymer spinning solution to prepare MOF membranes that have both PM filtration and pollution gas adsorption capacity.[21–23] However, the preparation process is difficult, and MOFs are encapsulated by the polymer, decreasing the adsorption capacity. Although many studies have been conducted and great progress has been made in preparing materials with an improved gas adsorption capacity,[24–28] the ability to selectively adsorb toxic gases present at low concentrations remains an elusive goal. There is urgency to prepare a material which can adsorb gases to meet WHO air quality standards. It is also especially important to eliminate the interference of other gases in the atmosphere and selectively adsorb toxic gases.

There are several mechanisms for MOFs to adsorb gases selectively. (a) The pore size of MOFs could potentially be controlled to facilitate the adsorption of gas molecules with different sizes. (b) The type of organic ligands, the specific electrostatic force, hydrogen bonds, and dipole–dipole interactions between ligands and gases could provide a possibility for selective adsorption. (c) The presence of metal and open metal sites with which electron-rich molecules could potentially interact presents a further possibility.[19,20,29,30] Therefore, it is important to choose suitable ligands according to the properties of the gases. Herein, we fabricate MIL-53(Al)-NH_2 onto the surface of a polyacrylonitrile (PAN) electrospun membrane by a hydrothermal process to prepare an MOF-based fibrous membrane. In accordance with the weak acidity of SO_2 and strong oxidative ability of O_3, we chose 2-aminoterephthalic acid as an organic ligand, which has basic functional groups and a reductive matrix to achieve selective adsorption through chemical action. MIL-53(Al)-NH_2 grown on PAN (MGP) fibrous membranes possess an excellent adsorption capacity for PM, SO_2, and O_3.

Results and discussion

Characterization of fibrous membranes

Fig. 1a shows the method used for MIL-53(Al)-NH_2@PAN (MGP) fibrous membrane fabrication. As shown in Fig. 1b, many filaments intertwined to form a porous PAN fibrous membrane, with a thickness of approximately 59 μm. After Al^{3+} was coordinated to H_2BDC-NH_2 to form MOFs on the surface of the PAN fibrous membrane, the MGP fibrous membranes could effectively prevent PM and the MOFs could adsorb or react with toxic gases, such as SO_2 and O_3, because of their large specific surface area and reactive organic ligands (Fig. 1c and d).

We also prepared 30 wt% and 60 wt% fibrous membranes as controls by adding MIL-53(Al)-NH_2 to a PAN solution before electrospinning. Fig. 2a–d show the morphology of fibrous membranes detected using SEM. With the addition of the MIL-53(Al)-NH_2 sheet (Fig. S1†), the diameter of the fibers increased gradually from approximately 400 nm to 500 nm and eventually to 600 nm. The MOFs altered the surface structure and area of the fibers. The surfaces of the PAN fibers were all very smooth. After adding 30 wt% MOF, the surfaces of the fibers became rough and the diameters of the fibers decreased, which indicated that MIL-53(Al)-NH_2 increased the force of the PAN solution in the electrostatic field. In 60 wt% MOF added PAN fibrous membranes, the surfaces of the fibers became coarser due to the presence of a large number of MOFs. Specifically, a layer of flaky MOFs grew on the surface of the MGP fibers. Energy-dispersive X-ray spectrometry (EDS) results also indicated a uniform deposition of the MOFs in the fibers. Fig. 2e shows the content of aluminum, which could also represent the amount of MIL-53(Al)-NH_2 in the various fibrous membranes. The content of the MOFs in the MGP

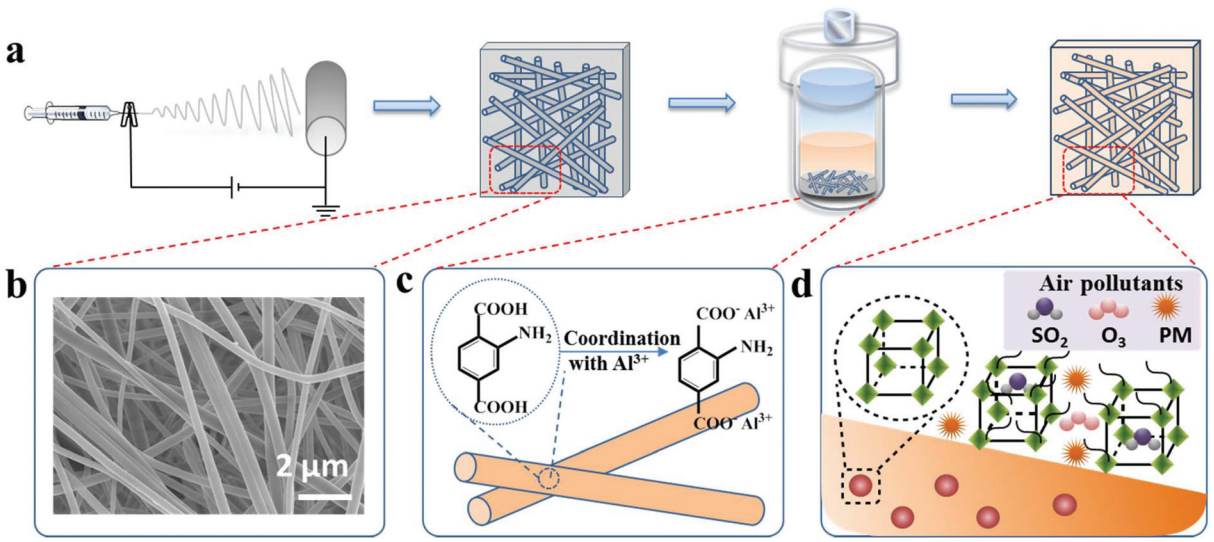

Fig. 1 The preparation and adsorption processes of MOF-based fibrous membranes. (a) Schematic diagram. (b) SEM image of PAN fibrous membranes. (c) The principle of the complexation reaction between Al^{3+} and H_2BDC-NH_2. (d) The adsorption of PM and the capture of toxic gases by MOF-based fibrous membranes.

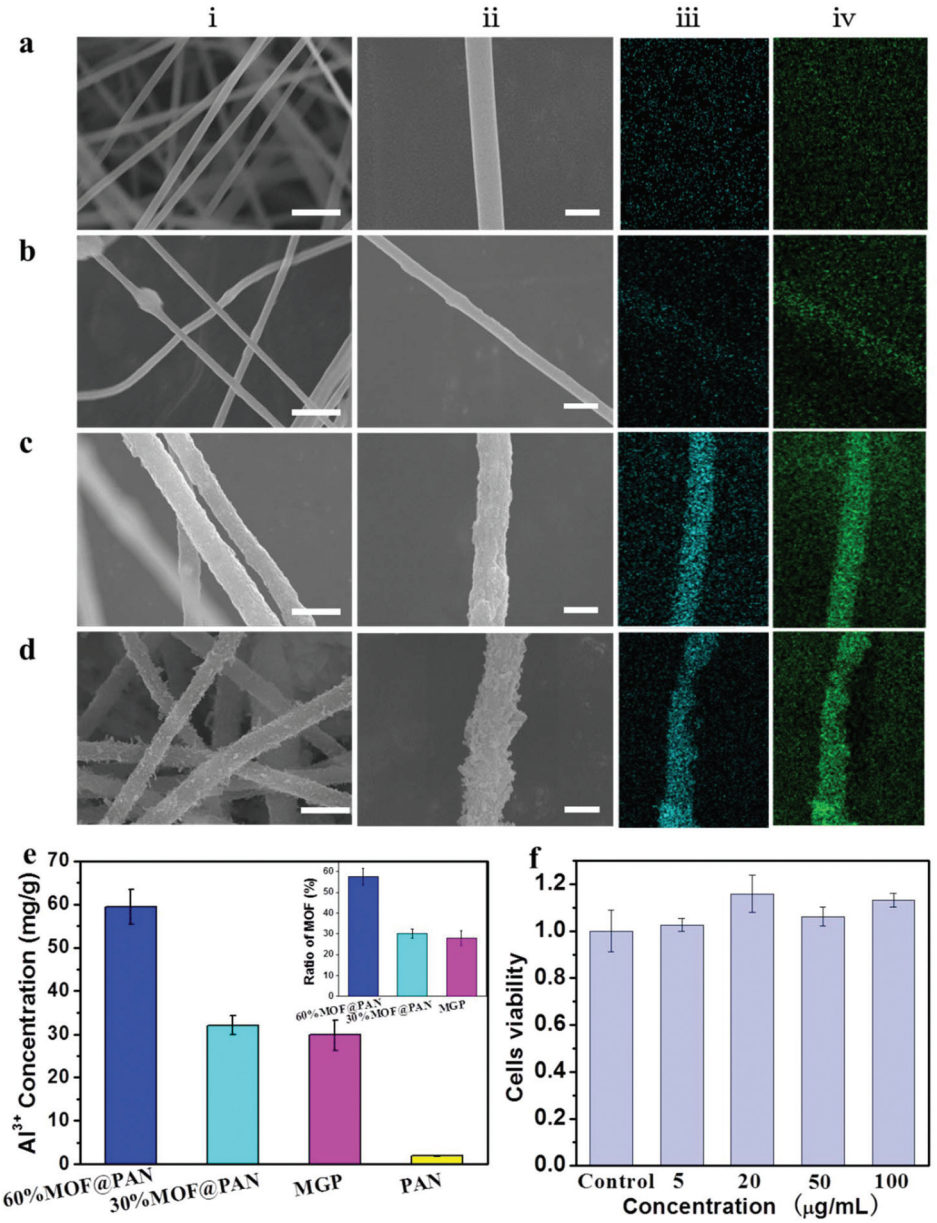

Fig. 2 Characterization of nanofibrous membranes. (a–d) SEM images of PAN (a), 30% MIL-53(Al)-NH_2@PAN (b), 60% MIL-53(Al)-NH_2@PAN (c), MGP (d). Scale bars represent 2 μm (i) and 500 nm (ii). X-ray EDS was used to detect Al^{3+} (iii) and O (iv). (e) ICP-OES was used to detect the concentration of Al^{3+}. Inset: The content of MOFs according to the concentration of Al^{3+}. (f) Cell viability was measured using the CCK-8 assay.

fibrous membranes was similar to that of the 30%MOF@PAN fibrous membranes. Each gram of the PAN membrane could load 0.33 g MIL-53(Al)-NH_2, which was considered a high loading capacity.

MGP fibrous membrane had an excellent adsorption capacity for PM

The adsorption efficiency of the various fibrous membranes was investigated in a heavily polluted environment in Beijing (Fig. 3). Except for the commercial-1, the adsorption efficiencies of the other membranes were all in excess of 99%, especially the MGP fibrous membrane, which reached an efficiency of 99.99% (Fig. 3a). After adsorbing PM, a large number of particles adhered to the surface of the fibers (Fig. S2†). The excellent adsorption performance may be attributed to the following characteristics:[31] (1) PM, with C–H, C═O, O–H, C═C, C–N and C–O functional groups, showed dipole–dipole interactions with polymers and with MIL-53(Al)-NH_2 of the fibrous membranes; (2) the fibers were intertwined to form a number of small holes with large surface areas, which enabled the physical adsorption of the particles.

To evaluate the long-term adsorption capacity of the MGP fibrous membranes, a vacuum pump was connected to the MGP fibrous membranes for 7 days, 15 h a day. The adsorption

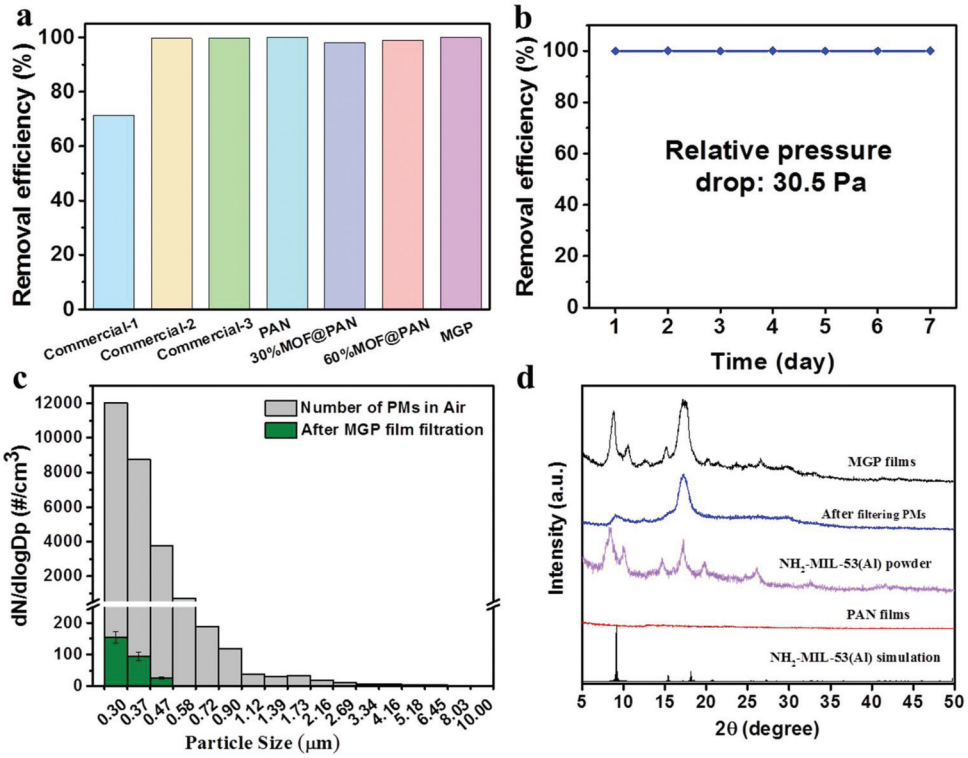

Fig. 3 MOF-based nanofibrous membranes had an excellent adsorption capacity for PM. (a) The real-time removal efficiency of various fibrous membranes for PM. (b) The removal efficiency of MGP fibrous membranes for PM. MGP fibrous membranes were connected to a pump with a pipe, which worked continuously to pump air at a rate of 3 L min^{-1} for 15 h per day. After 7 days, the removal efficiencies of PM were measured. (c) The number of PM of different sizes detected using OPS before and after adsorption by MGP fibrous membranes. (d) XRD patterns of the various fibrous membranes.

efficiency was tested every day and remained at 99.99%. After 7 days, the MGP fibrous membranes still showed excellent adsorption ability with a relative pressure drop of only 30.5 Pa (Fig. 3b). $PM_{2.5}$ and PM_{10} represent PM with a diameter less than 2.5 μm and 10 μm, respectively. In fact, fine particles (diameter <2.5 μm) are also very important pollutants and more likely to deposit in the lungs through the respiratory tract and subsequently diffuse into capillaries. The MGP membrane also has a high filtration effect (>99%) for fine particles (300 nm, Fig. 3c). The characteristic peaks in XRD patterns proved that MIL-53(Al)-NH_2 was generated on the surface of the PAN films successfully. After filtering PM, the crystal structure of the MGP fibrous membranes was damaged slightly that may be due to the interaction between the functional group of MIL-53 (Al)-NH_2 and the polar functional group of PM (Fig. 3d).

MOF-based nanofibrous membranes had a rapid and excellent adsorption capacity for SO_2

To investigate the adsorption capacity of various fibrous membranes, we designed an experimental device (Fig. 4a). SO_2 and N_2 were rapidly mixed in the mixing chamber and passed through the fibrous membranes at a speed of 700 mL min^{-1}. Three types of commercially available membranes were used as controls. The initial concentration of SO_2 was 7300 ppb. After the mixed gases passed through the MGP membrane, the concentration of SO_2 dropped rapidly to 40 ppb, while it remained at 5000–7000 ppb when other membranes were used (Fig. 4b). Furthermore, to test whether other gases in the environment, such as CO_2 and O_2, affected the adsorption capacity, we replaced nitrogen with atmospheric gases. It was apparent that the MGP membrane maintained a rapid and excellent adsorption capacity for SO_2 (Fig. 4c). Specifically, the adsorption capacity of the MGP fibrous membranes (2.8 mg g^{-1}) was 20 times that of the 30%MOF@PAN fibrous membranes (0.14 mg g^{-1}), which contained MOFs at the same concentration. As shown in Fig. S3† and Fig. 4b, the SO_2 adsorption capacity of MIL-53(Al)-NH_2 powder was slightly higher than that of the MGP films. The active sites, such as open metal sites or alkaline functional groups, must be fully exposed to toxic gases to increase the selective adsorption capacity of MIL-53(Al)-NH_2.

After the MGP fibrous membranes adsorbed SO_2 to saturation, thermogravimetric mass spectrometry (TG-MS) was used to measure the adsorption behavior. Gases generated during the pyrolysis process were detected using a mass spectrometer. The green line in Fig. 4d represents the relative content of SO_2. SO_2 spillover could be detected when the temperature was higher than 150 °C, which could be considered a form of physical adsorption. When the temperature reached 330 °C, there was a rapid release of SO_2. At the same time, the mass

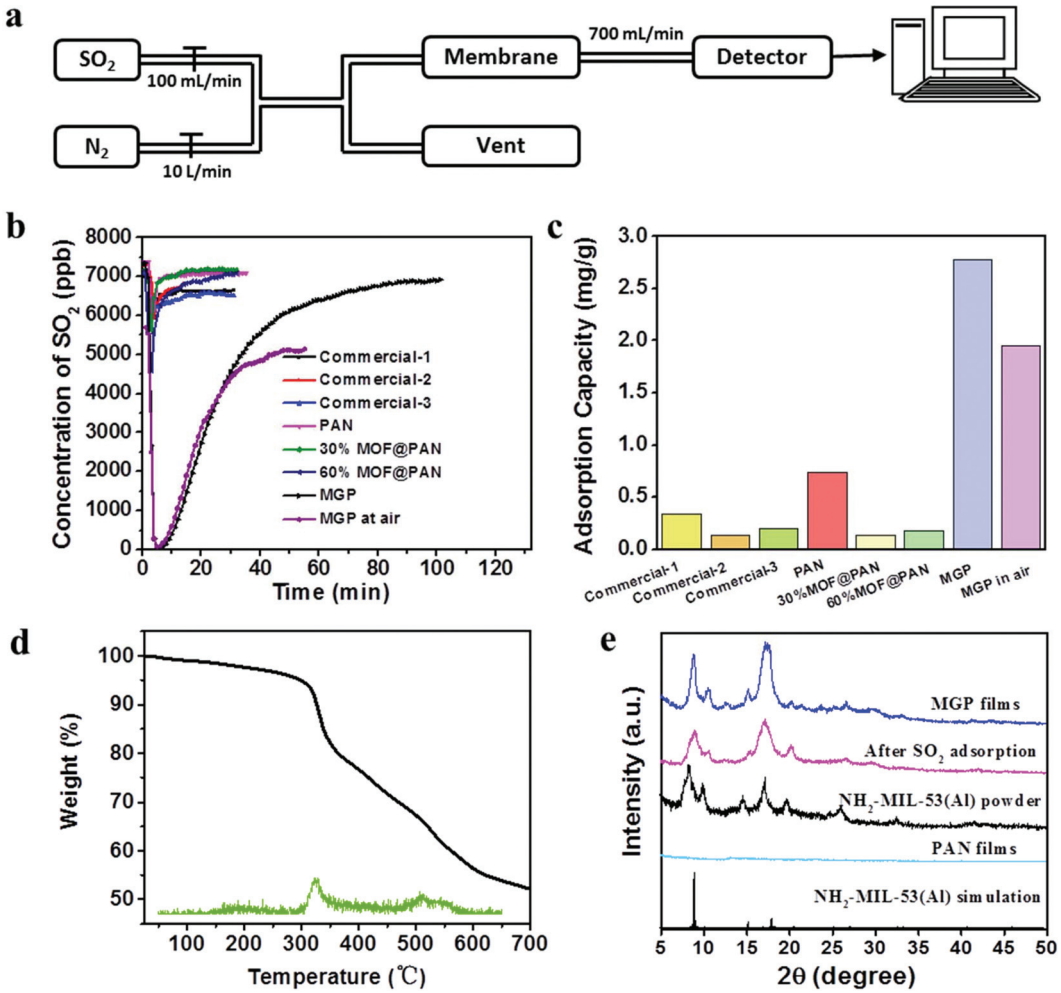

Fig. 4 MOF-based nanofibrous membranes had a rapid and excellent adsorption capacity for SO_2. (a) Schematic diagram of the SO_2 adsorption process. (b, c) SO_2 adsorption capacity of the different fibrous membranes. (d) The concentration of SO_2 detected using TG-MS with an increase in temperature after the SO_2 adsorbed MGP fibrous membranes were heated. (e) XRD patterns of MGP fibrous membranes before and after SO_2 adsorption.

began to decline rapidly, which indicated that the material was decomposing and that the chemically adsorbed SO_2 was being released. The MGP membrane had both physical and chemical adsorption abilities for SO_2. The amino group as an alkaline functional group might interact with acidic gases, which would increase their ability to adsorb SO_2 preferentially. To investigate the change in the crystal structure of the MOFs during electrospinning and SO_2 adsorption, analysis of the structure of the fibrous membranes was conducted by XRD (Fig. 4e). The crystal structure of the MGP membranes changed slightly, which proved that the destruction of SO_2 on the crystal structure is not obvious.

MOF-based nanofibrous membranes had a rapid and excellent adsorption capacity for O_3

O_3, a reactive and strongly oxidizing gas, was successfully adsorbed by the MGP fibrous membranes. A high concentration of O_3 was prepared by ultraviolet irradiation of O_2 and diluted with N_2 (Fig. 5a). The diluted O_3 passed through the MGP membrane at a rate of 850 mL min^{-1} and was detected using an O_3 analyzer. The commercial membranes, PAN fibrous membrane, 30%MOF@PAN, and 60%MOF@PAN fibrous membranes quickly reached saturation in the O_3 environment (the initial concentration was 3000 ppb). However, it took 48 h for the MGP membrane to achieve saturation. More importantly, after passing through the fibrous membranes, the concentration of O_3 decreased from 3000 ppb to 7 ppb, which was far below the national air quality standards (81 ppb). Using the weight of the fibrous membranes and the purification curve, we calculated the purification capacity of the different fibrous membranes (Fig. 5b). Except for the MGP fibrous membranes, the other membranes showed low capacity for O_3 adsorption. As shown in Fig. S4† and Fig. 5c, the O_3 adsorption capacity of MIL-53(Al)-NH_2 powder was the same as that of the MGP films. N_2 was replaced with air, simulating the natural atmospheric environment to enable detection of the selectivity of the MGP fibrous membranes to O_3 (Fig. 5b and c). The removal capacity of the

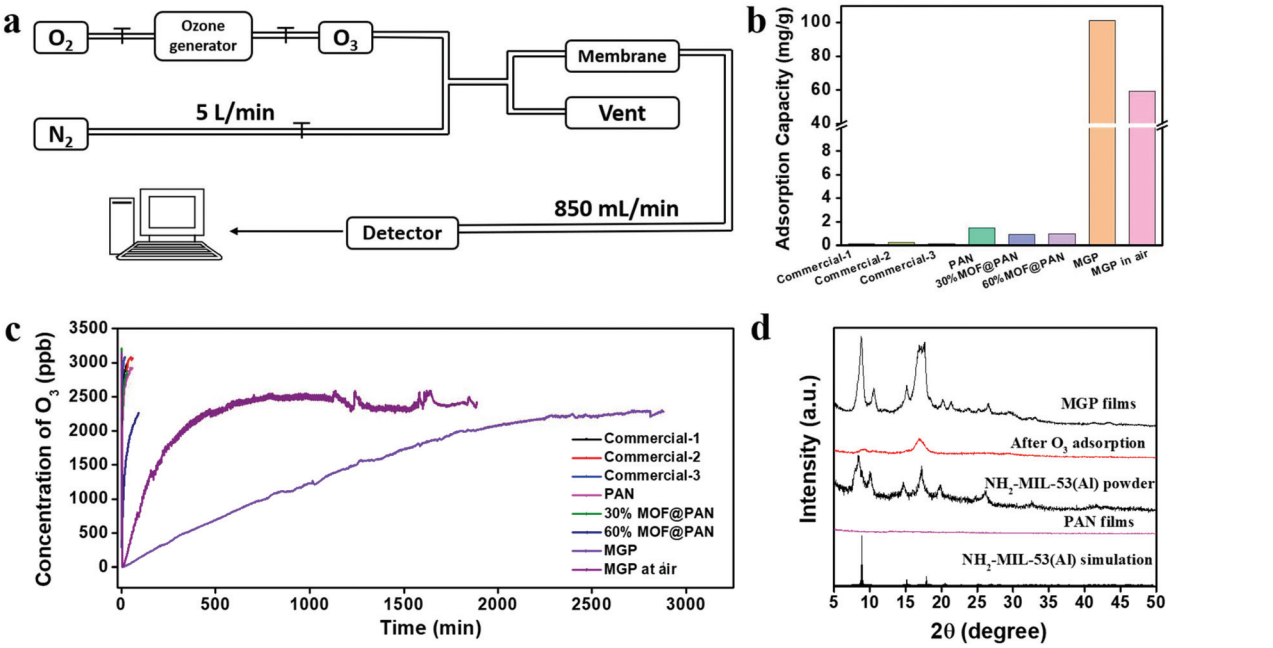

Fig. 5 MOF-based nanofibrous membranes had a rapid and excellent adsorption capacity for O_3. (a) Schematic diagram of the O_3 adsorption process. (b, c) O_3 adsorption capacity of the different fibrous membranes. (d) XRD patterns of MGP fibrous membranes before and after O_3 adsorption.

MGP fibrous membranes for O_3 remained excellent. Other gases in the air did not significantly affect the O_3 removal capacity. XRD results showed that the crystal structure of MIL-53(Al)-NH_2 was destroyed after it reacted with O_3 (Fig. 5d).

To further illustrate the mechanism of the reaction between O_3 and MIL-53(Al)-NH_2, IR spectroscopy was used to characterize the change in chemical bonds before and after O_3 adsorption. We synthesized pure MIL-53(Al)-NH_2 to which we did not add PAN fibrous membranes, and exposed it to a high concentration of O_3 (Fig. S5a†). After treatment with O_3, the position and intensity of the peaks in the infrared spectra changed significantly. The peak at 1575 cm^{-1} represents the amino group on the benzene ring. After reacting with O_3, the peak position shifted to 1629 cm^{-1}, which represents the azo and nitroso groups. Based on changes in the peaks and the available literature,[32,33] we speculate that the following reactions may occur (Fig. 6): (1) upon oxidation by O_3, two molecules of 2-aminoterephthalic acid were condensed by the amino group to form an azo bond; (2) the amino group was oxidized to an imine by O_3; (3) the amino group as an *ortho–para* directing group and the carboxyl group as a *meta* directing group led to the *para*-position of the amino group becoming a highly reactive site, which easily reacted with O_3 to form a phenol; and (4) aniline was oxidized to benzoquinone. These possible chemical reactions depended on the unique oxidation potential of O_3 and endowed the membrane with the ability to adsorb O_3 selectively.

Interestingly, we mixed all the raw materials which were used to synthesize MIL-53(Al)-NH_2 and repeated the above steps. Fourier transform infrared spectroscopy (FTIR) showed

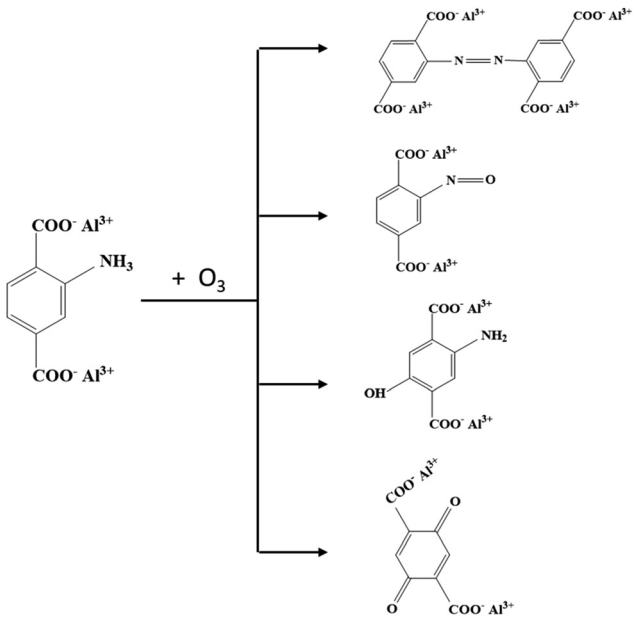

Fig. 6 Possible chemical reactions between O_3 and MIL-53(Al)-NH_2.

that there was almost no change in the peaks before and after exposure to O_3, which suggests that raw materials cannot react with O_3 in a fast-flowing environment (Fig. S5b†). This observation provides strong proof that the structure or the complexation of aluminum and organic ligands promotes the reaction. It is possible that the porous structure provides a sufficient reaction time after adsorption of O_3 or aluminum

ions to reduce the distance between the two ligands and act as a catalyst. MIL-53(Al)-NH_2 and raw materials (aluminum nitrate nonahydrate and 2-aminoterephthalic acid) were also treated with O_3 at a concentration of 3070 ppb, and the O_3 concentration was measured after passing through the materials (Fig. S6†). The raw materials barely absorbed O_3 compared with MIL-53(Al)-NH_2, which caused the concentration to drop from 3070 ppb to 10 ppb rapidly. The result was also confirmed by a shift in the position of the IR peak.

Conclusions

In summary, we combined the physical and chemical properties of a toxic gas to select appropriate organic ligands and prepared MOF-based fibrous membranes, which had an excellent ability to adsorb PM and toxic gases selectively. The removal efficiency of the MGP fibrous membranes for PM could reach 99.99% even for the finer PM (about 300 nm). More importantly, under low partial pressure and complex gas composition conditions, the MGP fibrous membrane was able to selectively adsorb SO_2. The concentration of SO_2 dropped from 7300 ppb to 40 ppb. The MGP fibrous membrane had a very high purification capacity for O_3. The concentration of O_3 rapidly dropped from 3000 ppb to 7 ppb, which was far below the national air quality standards (81 ppb). Even under atmospheric conditions, the MGP fibrous membrane could adsorb toxic gases selectively, while not being influenced by the presence of other gases, such as CO_2 and O_2. The simple and inexpensive electrospinning technique and the MOF-based fibrous membranes have wide practicability in the field of environmental protection and air cleaning, among others.

Experimental

Chemicals and materials

2-Aminoterephthalic acid (H_2BDC-NH_2, 99%) was purchased from Alfa Aesar. Aluminum nitrate nonahydrate ($AlNO_3{\cdot}9H_2O$, 99%) and polyacrylonitrile (PAN, average M_w 150 000) were purchased from Macklin. Cetyl trimethyl ammonium bromide (CTAB, high purity grade) was purchased from Amresco. Tetramethylammonium hydroxide solution (25% methanol solution) was purchased from Aladdin. *N*,*N*-Dimethyl formamide (DMF), ethanol, and methanol were purchased from Beijing Chemical Works. All chemicals were used with no further purification.

Preparation of MIL-53(Al)-NH_2

MIL-53(Al)-NH_2 was synthesized according to a previously published study.[34] Briefly, 0.56 g H_2BDC-NH_2 was added to a 100 mL Teflon-lined stainless-steel autoclave with 10 mL deionized H_2O and 4 mL tetramethylammonium hydroxide solution. $AlNO_3{\cdot}9H_2O$ (1.68 g), 0.8 g CTAB, and 20 mL deionized H_2O were added to another 100 mL autoclave. Next, both autoclaves were sealed and heated at 100 °C for 1 h in an oven. After cooling to room temperature, the solutions in the autoclaves were mixed and transferred to another autoclave and heated at 100 °C for 16 h. The product was washed five times with deionized H_2O and ethanol and dried under vacuum at room temperature.

Electrospinning

The process of electrospinning was based on a previously published study.[14,35] PAN (1.4 g) was dissolved in 10 mL DMF and stirred overnight at room temperature. Then, 2.1 g MIL-53(Al)-NH_2 was added to a 14% PAN solution with constant stirring to obtain a yellow solution which contained 60 wt% MOF. Subsequently, 30 wt% MOF@PAN was prepared using the same method.

The PAN/DMF solution was loaded into a 10 mL syringe and then transferred to the electrospinning unit at 25 kV. The propulsion speed was 0.006 mm s^{-1}, and the spinneret diameter was 0.6 mm. The distance between the spinneret and the collecting roller was 20 cm, and the spinning time was 2 h.

Incorporation of MIL-53(Al)-NH_2 into the electrospinning PAN fiber

Solution 1 was prepared according to the following procedure. H_2BDC-NH_2 (0.56 g) was dissolved in 10 mL H_2O, which contained 4 mL tetramethylammonium hydroxide, and then transferred to a 100 mL Teflon-lined stainless-steel autoclave. Then, an as-spun PAN membrane was immersed in an as-prepared solution at 100 °C for 1 h.

Solution 2 was prepared according to the following procedure. $AlNO_3{\cdot}9H_2O$ (1.68 g) and 0.8 g CTAB were dissolved in 20 mL deionized H_2O in a 100 mL autoclave at 100 °C for 1 h.

After cooling to room temperature, solution 2 was poured into solution 1 to obtain a white flocculent mixture, which was sealed and heated at 100 °C for 16 h. After completion of the reaction, the fibrous membranes were washed with deionized H_2O and absolute ethanol five times, separately. Then, the fibrous membranes were dried at 60 °C.

Characterization

The ultrastructure and surface morphology of various fibrous membranes were characterized using transmission electron microscopy (TEM, Tecnai G2 20 S-TWIN) and scanning electron microscopy (SEM, Hitachi S4800). The chemical composition of various fibrous membranes was characterized by energy-dispersive X-ray spectrometry (EDS, Hitachi-SU8220-EDS). The concentration of Al^{3+} was measured using inductively coupled plasma–optical emission spectroscopy (ICP-OES, Shimadzu, Kyoto, Japan). The crystalline structure of various fibrous membranes was analyzed using X-ray diffraction (XRD) spectroscopy with a Cu Kα radiation source at 40 kV and 30 mA. The weightlessness process and chemical composition of the materials were characterized by thermogravimetric mass spectrometry (TG-MS). Fourier transform infrared spectroscopy (FTIR, Spotlight 200i) was used to analyze the chemical structure. SO_2 and O_3 were detected using a gas analyzer (43i-DNSAB, APIT400).

Cytotoxicity assay

The cytotoxicity of MIL-53(Al)-NH_2 at different concentrations (5, 20, 50, 100 μg mL^{-1}) was tested using a cell count kit-8 assay (CCK-8) (Kumamoto Techno Research Park, Japan). Human epithelial cells were cultured in DMEM containing 10% fetal bovine serum and 1% penicillin–streptomycin. MIL-53(Al)-NH_2 at different concentrations of 5, 20, 50 and 100 μg mL^{-1} was added to a 96-well plate to incubate the cells for 24 h. Next, the cells were washed 3 times using PBS, and 10 μL CCK-8 solution was added to each well and incubated at 37 °C for 4 h. The absorbance was detected at 450 nm. Cell viability was calculated by the following formula:

$$\text{Cell viability}(\%) = \frac{A_i - A_0}{A_c - A_0} \times 100\%$$

where A_i represents the absorbance at different concentrations, A_c is the absorbance without the added MIL-53(Al)-NH_2, and A_0 is the absorbance of DMEM and CCK-8.

PM filtration and pressure drop of fibrous membranes

A hand-held condensation particle counter (CPC, TSI model 3007, USA) and an optical particle sizer (OPS, TSI model 3330, USA) were used to monitor the total number, concentration, and size distribution of the atmospheric PM. The measurement range of the particle size was 0.01 to 10 μm. Filtration efficiency was determined by measuring PM numbers before and after passage through the membranes. The CPC 3007 can pump at a constant rate. A filter with a diameter of 4 cm was set up on the front end of the pumping port. The PM removal efficiency was calculated using the following equation:

$$E = \frac{C_1 - C_2}{C_1}$$

where C_1 (particles per cm^3) and C_2 (particles per cm^3) are the particle number concentrations of particle matter with and without the filter, respectively, and E is the efficiency of PM removal.

The pressure drop, representing resistance across the air filter, was measured using a differential manometer.

SO_2 adsorption

Fig. 4a shows the adsorption process of SO_2. The flow rate of SO_2 was 100 mL min^{-1}, and the flow rate of N_2 was 10 L min^{-1}. SO_2 and N_2 were fully mixed in a pipe, and the concentration of SO_2 was 7300 ppb. Then, the gas mixture passed through five-layer membranes at a rate of 700 mL min^{-1} and was detected. The adsorption capacity was calculated using the following equations:

$$m_1 = C_0 \cdot r \cdot t$$

$$m_2 = \int_0^t C_0 \cdot r \cdot \mathrm{d}t$$

$$\text{Capacity} = \frac{m_1 - m_2}{m_0}$$

where C_0 (mg m^{-3}) is the initial concentration, r (m^3 min^{-1}) is the flow rate of the mixture, t (min) is the test time, m_1 (mg) is the total mass of SO_2 in the test time, m_2 (mg) is the area of the adsorption curve, and m_0 (mg) is the weight of the membrane.

O_3 adsorption

Fig. 5a shows the experimental procedure, which was similar to the SO_2 adsorption test. Briefly, O_2 flowing at a velocity of 50 mL min^{-1} passed through the O_3 generator to obtain a high concentration of O_3 which was diluted by nitrogen with a flow rate of 5 L min^{-1}. The gas mixture passed through a five-layer fibrous membrane at a flow rate of 850 mL min^{-1} and was detected. The adsorption capacity was calculated using the above formulas. When air was used as the diluted gas, the flow rate was changed to 670 mL min^{-1} and the gas mixture was passed through a three-layer fibrous membrane.

Conflicts of interest

There are no conflicts to declare.

Acknowledgements

This work was financially supported by the National Science Fund for Excellent Young Scholars (31622026), the Key Program for International S&T Cooperation Projects of China (2016YFE0133100), the Science Fund for Creative Research Groups of the National Natural Science Foundation of China (11621505), the National Natural Science Foundation of China (21876205, 11435002, 91543206) and the National Basic Research Program of China (2017YFC1600204, 2016YFA0201600, and 2016YFA0203204).

References

1 C. A. Pope 3rd, R. T. Burnett, G. D. Thurston, M. J. Thun, E. E. Calle, D. Krewski and J. J. Godleski, *Circulation*, 2004, **109**, 71–77.
2 L. C. C. Tracy, A. Kimmel, M. C. Bosland and C. Nadziejko, *Toxicol. Appl. Pharmacol.*, 1997, **144**, 348–355.
3 X.-Y. Z. Wei-Jie Guan, K. F. Chung and N.-S. Zhong, *Lancet*, 2016, **388**, 1939.
4 M. L. Block and L. Calderon-Garciduenas, *Trends Neurosci.*, 2009, **32**, 506–516.
5 B. A. Maher, I. A. Ahmed, V. Karloukovski, D. A. MacLaren, P. G. Foulds, D. Allsop, D. M. Mann, R. Torres-Jardon and L. Calderon-Garciduenas, *Proc. Natl. Acad. Sci. U. S. A.*, 2016, **113**, 10797–10801.
6 J. A. Bernstein, N. Alexis, C. Barnes, I. L. Bernstein, J. A. Bernstein, A. Nel, D. Peden, D. Diaz-Sanchez, S. M. Tarlo and P. B. Williams, *J. Allergy Clin. Immunol.*, 2004, **114**, 1116–1123.
7 M. Fernando Holguin, *Immunol. Allergy Clin. North Am.*, 2008, **28**, 577–588.

8 F. Zhu, R. Ding, R. Lei, H. Cheng, J. Liu, C. Shen, C. Zhang, Y. Xu, C. Xiao, X. Li, J. Zhang and J. Cao, *Respir. Med.*, 2019, **146**, 57–65.
9 H. Guo and M. Chen, *Ecotoxicol. Environ. Saf.*, 2018, **161**, 184–189.
10 A. Havet, F. Zerimech, M. Sanchez, V. Siroux, N. Le Moual, B. Brunekreef, M. Stempfelet, N. Kunzli, B. Jacquemin, R. Matran and R. Nadif, *Eur. Respir. J.*, 2018, **51**, 1702036–1702046.
11 X. Li, L. Huang, N. Wang, H. Yi and H. Wang, *Toxicol. Lett.*, 2018, **285**, 43–50.
12 C. Sack, S. Vedal, L. Sheppard, G. Raghu, R. G. Barr, A. Podolanczuk, B. Doney, E. A. Hoffman, A. Gassett, K. Hinckley-Stukovsky, K. Williams, S. Kawut, D. J. Lederer and J. D. Kaufman, *Eur. Respir. J.*, 2017, **50**, 1700559–1700568.
13 J. Xu, C. Liu, P. C. Hsu, K. Liu, R. Zhang, Y. Liu and Y. Cui, *Nano Lett.*, 2016, **16**, 1270–1275.
14 M. Guo, G. Zhou, Z. Liu, J. Liu, J. Tang, Y. Xiao, W. Xu, Y. Liu and C. Chen, *Sci. Bull.*, 2018, **63**, 92–100.
15 F. Kayaci, S. Vempati, C. Ozgit-Akgun, I. Donmez, N. Biyikli and T. Uyar, *Nanoscale*, 2014, **6**, 5735–5745.
16 A. Camposeo, L. Persano and D. Pisignano, *Macromol. Mater. Eng.*, 2013, **298**, 487–503.
17 R. Freund, U. Lachelt, T. Gruber, B. Ruhle and S. Wuttke, *ACS Nano*, 2018, **12**, 2094–2105.
18 H. Furukawa, K. E. Cordova, M. O'Keeffe and O. M. Yaghi, *Science*, 2013, **341**, 1230444.
19 J. R. Li, R. J. Kuppler and H. C. Zhou, *Chem. Soc. Rev.*, 2009, **38**, 1477–1504.
20 S. X. Banglin Chen and G. Qian, *Acc. Chem. Res.*, 2010, **43**, 1115–1124.
21 A. X. L. Gregory, W. Peterson and T. H. Epps III, *ACS Appl. Mater. Interfaces*, 2017, **9**, 32248–32254.
22 X. Lu, M. McEntee, M. A. Browe, M. G. Hall, J. B. DeCoste and G. W. Peterson, *ACS Appl. Mater. Interfaces*, 2017, **9**, 13632–13636.
23 W. T. Koo, S. J. Choi, S. J. Kim, J. S. Jang, H. L. Tuller and I. D. Kim, *J. Am. Chem. Soc.*, 2016, **138**, 13431–13437.
24 C. Liu, Y. N. Wu, C. Morlay, Y. Gu, B. Gebremariam, X. Yuan and F. Li, *ACS Appl. Mater. Interfaces*, 2016, **8**, 2552–2561.
25 R. Ostermann, J. Cravillon, C. Weidmann, M. Wiebcke and B. M. Smarsly, *Chem. Commun.*, 2011, **47**, 442–444.
26 X. J. Huixin Liang, C. Li and D. Chen, *J. Mater. Chem. A*, 2018, **6**, 334.
27 R. W. Ye Bian, S. Wang, C. Yao, W. Ren, C. Chen and Li Zhang, *J. Mater. Chem. A*, 2018, **6**, 15807.
28 Y. Zhang, Y. Zhang, X. Wang, J. Yu and B. Ding, *ACS Appl. Mater. Interfaces*, 2018, **10**, 34802–34810.
29 D. Britt, D. Tranchemontagne and O. M. Yaghi, *Proc. Natl. Acad. Sci. U. S. A.*, 2008, **105**, 11623–11627.
30 M. R. Tchalala, P. M. Bhatt, K. N. Chappanda, S. R. Tavares, K. Adil, Y. Belmabkhout, A. Shkurenko, A. Cadiau, N. Heymans, G. De Weireld, G. Maurin, K. N. Salama and M. Eddaoudi, *Nat. Commun.*, 2019, **10**, 1328.
31 C. Liu, P. C. Hsu, H. W. Lee, M. Ye, G. Zheng, N. Liu, W. Li and Y. Cui, *Nat. Commun.*, 2015, **6**, 6205.
32 J. Zhang, Y. Wu, C. Qin, L. Liu and Y. Lan, *Chemosphere*, 2015, **141**, 258–264.
33 A. Tekle-Rottering, C. von Sonntag, E. Reisz, C. V. Eyser, H. V. Lutze, J. Turk, S. Naumov, W. Schmidt and T. C. Schmidt, *Water Res.*, 2016, **98**, 147–159.
34 A. Pustovarenko, M. G. Goesten, S. Sachdeva, M. Shan, Z. Amghouz, Y. Belmabkhout, A. Dikhtiarenko, T. Rodenas, D. Keskin, I. K. Voets, B. M. Weckhuysen, M. Eddaoudi, L. de Smet, E. J. R. Sudholter, F. Kapteijn, B. Seoane and J. Gascon, *Adv. Mater.*, 2018, **30**, e1707234.
35 W. Xu, M. Guo, J. Liu, Y. Xiao, G. Zhou, Y. Liu and C. Chen, *J. Biomed. Nanotechnol.*, 2018, **14**, 179–189.